Construction of Defect-Diminished Fatty Acid Langmuir–Blodgett Film and Its Optical Waveguide Properties

Masami Yanagida, Atsushi Takahara, and Tisato Kajiyama*

Department of Materials Physics and Chemistry, Graduate School of Engineering, Kyushu University, 6-10-1 Hakozaki, Higashi-ku, Fukuoka 812-8581

(Received July 13, 1999)

A Langmuir–Blodgett (LB) film for a optical planar waveguide with a low optical propagation loss could be constructed from highly organized fatty acid monolayers prepared by a cooling multi-step creep method. The cooling multi-step creep method is the novel preparation technique to form a defect-diminished monolayer on the water surfaces on the basis of both the structural relaxation induced by area-creep and the control of thermal molecular motions in the monolayer. The fatty acid monolayer prepared by the cooling multi-step creep method was morphologically homogeneous and mechanically stable, even at a high surface pressure where the monolayer prepared by a conventional continuous compression method easily collapsed. The crystallographical and structural regularities of the monolayer and the LB film prepared by the cooling multi-step creep method were remarkably improved, compared with those of the monolayer and the LB film prepared by the conventional continuous compression method. The LB film waveguides prepared by the cooling multi-step creep method were morphologically homogeneous and structurally regular and could propagate incident light with a low optical propagation loss.

In recent years, the optical waveguides constructed by organic materials have been attracting attention for the applications in integrated optical components because of the large non-linear optical properties of the organic materials.[1—5] Fabrication of the organic thin film is one of the most important processes for the realization of the integrated optical devices. The Langmuir–Blodgett (LB) technique, which is the preparation method of the organic thin film by the successive deposition of the monolayers on the water surface onto a solid substrate, can control the thickness and the structure of the organic thin film at a molecular level. Hence, it can be considered that the LB technique is quite effective for the construction of an organic thin film which is applied for the integrated optical components. However, the large loss of propagating light intensity in the LB film waveguides prevented the LB film from wide-ranging applications for the optical waveguides.[6,7] It can be considered that the large propagation loss of the LB film waveguides is caused by the morphological and structural inhomogeneity of the LB film, such as the interlayer roughness, the molecular defects and the irregular packing of the molecules in the LB film.

For the construction of the highly structurally regularized monolayers as the constituent unit of the LB film, it is necessary to investigate the aggregation state in the monolayer on the water surface. Previously, it has been reported that a defect-diminished fatty acid crystalline monolayer can be constructed by a multi-step creep method based on the area-creep characteristics.[8,9]

In this study, the cooling multi-step creep method was discussed from the viewpoints of both the thermal molecular motion and the structural relaxation in the monolayer, in order to prepare the highly structurally regularized monolayer. Furthermore, the highly structurally regularized LB film was constructed by the deposition of the structurally regularized monolayers. The optical waveguide properties of the LB film was studied on the basis of the TEM and atomic force microscopic (AFM) observations, X-ray scattering measurements and the propagation loss measurement, since such properties might reflect the relationships between propagation loss and structural regularity of the LB film waveguides.

Experimental

Monolayer Preparation. Stearic acid ($CH_3(CH_2)_{16}COOH$) with chromatographic reference quality was used without further purification. Benzene with spectroscopic quality was used as a spreading solvent. A benzene solution of stearic acid was prepared with a concentration of 3.0×10^{-3} mol dm^{-3} as a sample solution. The subphase water was purified with Milli-QII system (Millipore Co., Ltd.). The accuracy of the subphase temperature, T_{sp} was ±0.1 K which was evaluated by using a thermocouple. The dimensions of the trough were 400 mm in length, 150 mm in width and 5 mm in depth. The subphase water level was maintained by a home-made water level maintainer in order to prevent any decrease of the surface pressure due to the evaporation of the subphase water.[9] The surface pressure was measured by the Wilhelmy balance technique. Compression and area-creep measurements of the monolayer were carried out with a microprocessor-controlled film balance system (USI System Co., Ltd. FSD-20). The stearic acid monolayers were prepared by spreading 60 μl of the sample solution on the water surface, They were then compressed to the surface pressure of 24 mN m^{-1} with a constant compression speed of 120 mm^2 s^{-1} at T_{sp} of 293 K. In this study, since T_{sp} was below the crystalline relaxation temperature, T_{α_c} and the melting temperature, T_m of the stearic acid monolayer on the water surface (T_{α_c} = 298 K, T_m = 317 K),[10,11]

the stearic acid molecules formed the fusing-oriented crystalline monolayer, that is, the large-area mono-domain monolayer.[12]

Also, the crystalline monolayers of stearic acid were prepared by the multi-step creep[8,9] and the cooling multi-step creep method. In the case of the multi-step creep method, T_{sp} was controlled at 293 K. Scheme 1 shows the monolayer preparation process of the cooling multi-step creep method. The stearic acid monolayer was compressed up to the surface pressure of 3 mN m^{-1} at T_{sp} of 301 K above T_{α_c}, and then, maintained at the constant surface pressure. Then, the monolayer was further compressed to 5 mN m^{-1} and again, the monolayer was maintained at 5 mN m^{-1}. When the monolayer was compressed to the surface pressure of 7 mN m^{-1} and the sufficient area-creep at 7 mN m^{-1} was carried out, T_{sp} was cooled down to 293 K at a constant cooling speed of 1 K h^{-1} and the monolayer was simultaneously compressed to 10 mN m^{-1}. After repeating the similar process with an increase of the surface pressure, the monolayer was finally compressed to 24 mN m^{-1}. Finally, the stearic acid monolayers were transferred onto the solid substrate for various investigations, as described below.

Electron Microscopic Observation. The stearic acid monolayer on the water surface was transferred onto a hydrophilic SiO substrate by a horizontal drawing-up method[13] for TEM observation. The hydrophilic SiO substrate with a static contact angle (θ) of 30° for water was prepared by vapor deposition of SiO onto a glass slide on which an electron microscope grid of 200 mesh was covered with a collodion thin layer. It was confirmed from AFM (Seiko Instruments Industry Inc. SFA300) observation and electron diffraction (ED) study that the SiO substrate showed a smooth surface and was in the amorphous phase; also, the monolayer could be transferred onto the SiO substrate without any phase or crystallographical change.[11] Electron diffraction patterns of the monolayers were obtained by TEM (Hitachi H-7000), which was operated at an acceleration voltage of 75 kV and a beam current of a several μA. The electron beam was 10 μm in diameter. TEM observation was carried out at 293 K which corresponded to T_{sp}. The lateral crystallographical regularity, that is, the magnitudes of crystallographical distortion (D_{lat}) and continuity (L_{lat}), of the monolayers were evaluated by a single line method based on the Fourier analysis of the ED profiles.[14]

Spreading a sample on the water surface
T_{sp}=301 K ↓ Compression (60 mm^2 sec^{-1})
Area-creep (3 mN m^{-1})
↓ Compression (6 mm^2 sec^{-1})
Area-creep (5 mN m^{-1})
↓ Compression (6 mm^2 sec^{-1})
Area-creep (7 mN m^{-1})
Cooling to 293 K (1 K hour^{-1}) ↓ Compression to 10 mN m^{-1}
Area-creep (13 mN m^{-1})
↓ Compression (6 mm^2 sec^{-1})
Area-creep (15 mN m^{-1})
↓ Compression (6 mm^2 sec^{-1})
Area-creep (17 mN m^{-1})
↓ Compression (6 mm^2 sec^{-1})
Area-creep (20 mN m^{-1})
↓ Compression (6 mm^2 sec^{-1})
Area-creep (24 mN m^{-1})
↓
Transferred onto a substrate

Scheme 1. Preparation process of stearic acid monolayer by cooling multi-step creep method.

Small Angle X-Ray Scattering Measurement. The 30 monolayers were deposited onto a hydrophobic siliconized substrate (θ = 90° by a vertical dipping method for a small angle X-ray scattering (SAXS) measurement. The transfer ratios during this transferring process of the monolayers were always unity. The SAXS profiles of the LB films were obtained by an X-ray generator with a Kratky U-slit small angle X-ray diffractometer (Rigaku Rota Flex RU-300). An X-ray beam was generated with Cu $K\alpha$ radiation. SAXS measurement was carried out at a corresponding temperature to T_{sp} at which the LB films were prepared. From the SAXS profiles, a longitudinal structural regularity, that is, the magnitudes of longitudinal structural distortion (D_{long}) and longitudinal periodical continuity (L_{long}), of the LB films was evaluated based on Hosemann's paracrystal analysis.[15]

Atomic Force Microscopic Observation of the LB Film. The 30 monolayers were deposited onto a freshly cleaved mica (Okabe Mica Co., Japan) substrate by the vertical dipping method for AFM observation. The transfer ratios were always unity. AFM equipped with a 20 μm scanner and a Si_3N_4 tip on a cantilever with a spring constant of 0.02 N m^{-1} was employed for the surface morphological observation of the LB films. AFM observation was carried out under the "constant force" mode and at the temperature of 293 K at which the LB films were prepared. The applied force upon scanning was ca. 10^{-10} N. Under this scanning condition, the morphology of the LB films could be observed without any destruction of the film induced by scanning of the cantilever.

Measurement of Optical Propagation Losses from LB film Waveguides. The 149 monolayers were deposited onto a hydrophilic MgF_2 (θ = 50°) substrate by the vertical dipping method to construct the LB film waveguides. Figure 1(a) shows a schematic representation of the LB film waveguides on the MgF_2 substrate used in this study. In the case of a conventional method to evaluate the propagation loss of the LB film waveguides, an optical prism is directly pressed on the LB film, as shown in Fig. 1(b), and then the structure of the LB film is damaged by the pressure caused by the compression of the prism. Therefore, this structural change of the LB film waveguides makes the magnitude of propagation loss increased. Since, in the case of our homemade equipment as shown in Fig. 1(a), the optical prism with the refractive index (n) of 1.52 was fastened with the MgF_2 substrate (n = 1.38) for the coupling of an incident laser beam as shown in Fig. 1(a), the structure of the LB film waveguides did not suffer the propagation loss from setting the prism by using the newly developed substrate. As the refractive index of the LB film was 1.43, the incident light could propagate in the LB film by the total reflection at the interface among the LB film and air and the LB film and the substrate, respectively, because the refractive index of the LB film was larger than those of the substrate and air (n = 1.00). The optical propagation losses of the LB film waveguides were calculated from scattered light intensities from the LB film waveguides. Figure 2 shows the block diagram of a homemade experimental setup for the optical propagation loss measurements. A He–Ne laser beam was coupled into the LB film waveguide by a prism. The intensity of the scattered light from the LB film waveguides was detected by the movable photodiode

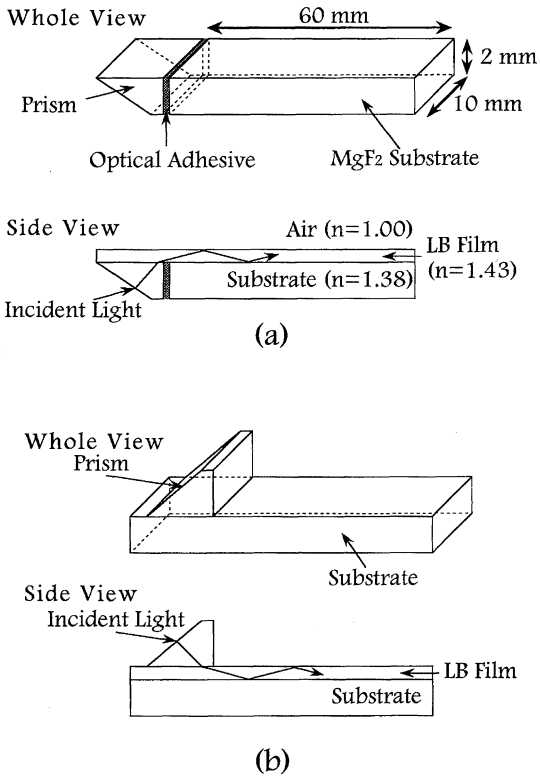

Fig. 1. Schematic representation of the substrate for propagation loss measurement. (a) was used in this study and (b) was used in conventional study.

whose position was controlled precisely along the direction of the light propagation in the waveguides.

Results and Discussion

Area-Creep Behavior of Stearic Acid Crystalline Monolayer at T_{sp} above T_{α_c}. Figure 3 shows the time dependence of the molecular occupied area for the stearic acid crystalline monolayer at various surface pressures at T_{sp} of 301 K. At this T_{sp}, the stearic acid monolayer forms a randomly assembled crystalline monolayer.[10—12] The surface pressure dependence of the area-creep behavior for the crystalline monolayer at T_{sp} above T_{α_c} was similar to that

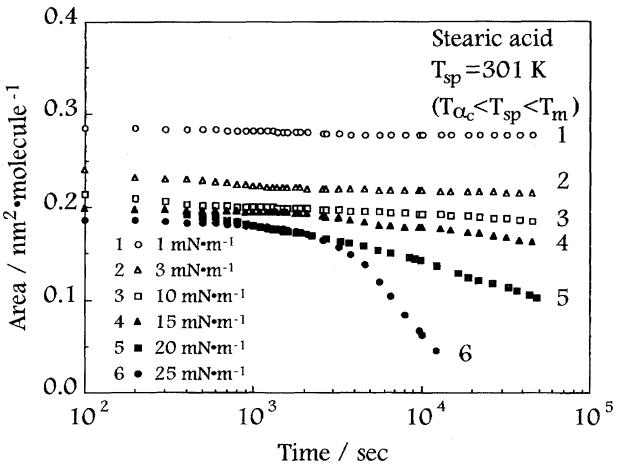

Fig. 3. Time dependences of the molecular occupied area for the stearic acid crystalline monolayer at various surface pressures at T_{sp} of 301 K.

of the crystalline monolayer at T_{sp} below T_{α_c}.[16] Hence, it seems reasonable to consider that the area-creep phenomena of the stearic acid crystalline monolayer at T_{sp} above T_{α_c} correspond to the structural and mechanical relaxation mechanisms at T_{sp} below T_{α_c}. The area-creep behavior for the stearic acid crystalline monolayer was roughly classified into two regions depending on the area-creep time, especially at the higher surface pressures, as shown by curves 5 and 6 of Fig. 3. In the case of a high surface pressure, the monolayer collapsed owing to a stress concentration at the macroscopic defects during the area-creep process for a long time, although stearic acid molecules in the crystalline domain were rearranged during the area-creep process for a short time. On the other hand, in the case of a low surface pressure as shown by curves 1 and 2 of Fig. 3, the area of the vacancies among the crystalline domains decreased and also the crystallographical regularity of the monolayer was remarkably progressed with an increase of area-creep time. Then, the area-creep behavior at a low surface pressure suggested one idea of how to prepare the defect-diminished monolayer.

Figure 4 shows the time dependence of the molecular oc-

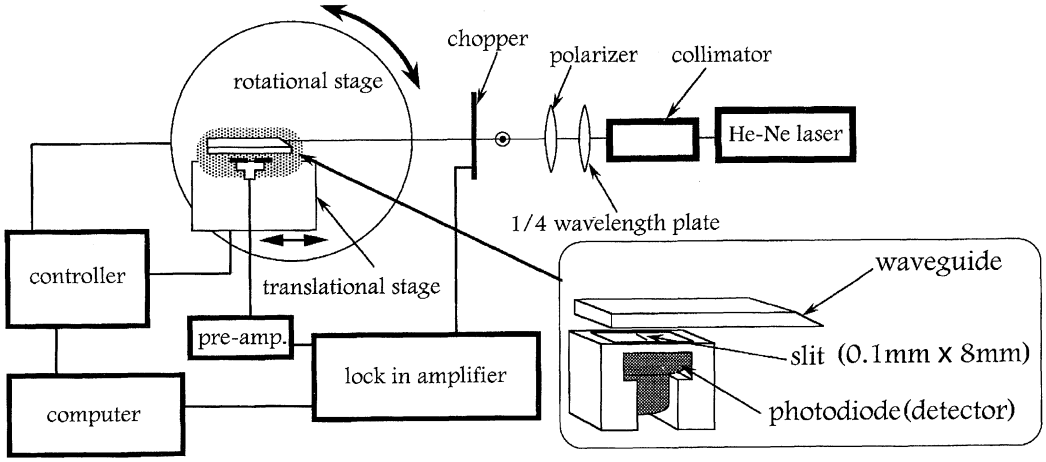

Fig. 2. Schematic setup for the home-made propagation loss measurement.

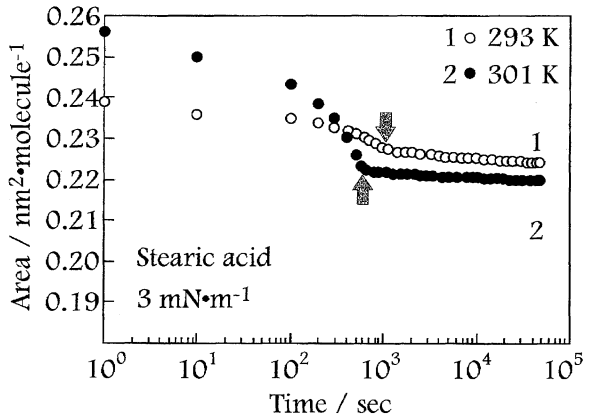

Fig. 4. Area-creep behavior for the stearic acid monolayer at the temperature of 293 K ($< T_{\alpha_c}$) and 301 K ($> T_{\alpha_c}$).

cupied area for the stearic acid crystalline monolayer at a low surface pressure of 3 mN m^{-1} at T_{sp} of 293 K below T_{α_c} and T_{sp} of 301 K above T_{α_c}. At both T_{sp} values, the surface area of the monolayer decreased gradually with an increase of creep time in a short area-creep time range, and finally, the surface area remained almost constant after the area-creep process indicated by the arrows in Fig. 4. Figure 4 indicates that the structural and mechanical relaxations of the monolayer were almost completed at the creep time indicated by the arrows. Since the magnitude of the creep time indicated by the arrow at T_{sp} of 301 K above T_{α_c} was shorter than that at T_{sp} of 293 K below T_{α_c}, the structural and mechanical relaxation proceeded faster at T_{sp} above T_{α_c} than those at T_{sp} below T_{α_c}. Furthermore, the molecular occupied area in the crystalline monolayer after a long area-creep time at 301 K was smaller than that at 293 K. The fast and high proceedings of the structural relaxation of the monolayer at T_{sp} above T_{α_c} is caused by the active thermal molecular motion of the molecules in the monolayer at T_{sp} above T_{α_c}. Therefore, it can be concluded from the results mentioned above that the area-creep of the crystalline monolayer at T_{sp} above T_{α_c} is more effective for the preparation of the highly structural regularized monolayer, based on the structural and mechanical relaxations.

Crystalline Monolayer Prepared by Cooling Multi-Step Creep Method. For the preparation of the highly structural regularized monolayer, it is necessary to compress the monolayer up to a high surface pressure, because the molecular packing in the monolayer is rearranged by sufficient compressing force. However, the stearic acid crystalline monolayer at T_{sp} above T_{α_c} cannot bear a surface pressure higher than 3 mN m^{-1}, as shown in Fig. 3, because the aggregation force among the molecules in the monolayer is weakened by the active thermal molecular motion of the stearic acid at T_{sp} above T_{α_c}. That is, the area-creep could not attain to the constant area with the creep time studied here, as shown by the curves 3—6. The cooling multi-step creep method as shown in Scheme 1 was proposed for the preparation of the highly structural regularized crystalline monolayers at a higher surface pressure.

Figure 5 shows the creep time dependence of molecular occupied area for the stearic acid crystalline monolayers at various surface pressures in the case of the multi-step creep method including a cooling process from 301 to 293 K. Since the molecular occupied area of the monolayer after a long creep time at 301 K and at the surface pressure of 3 mN m^{-1} could not reach a crystallographical area evaluated from its ED pattern (ca. 0.20 nm^2 molecule^{-1}), those results indicate that many vacancies and defects exist in the monolayer even after the area-creep at 3 mN m^{-1}. Furthermore, since the ED pattern of the stearic acid monolayer after a sufficient area-creep at T_{sp} above T_{α_c} showed crystalline Debye rings, it can be considered that the crystallites in the monolayer prepared at T_{sp} above T_{α_c} was randomly assembled without sintering at the interface among the crystalline domains.[11,12] Based on our previous report,[12] the monolayer should be cooling down to T_{sp} below T_{α_c} in order to obtain a large-area monodomain crystalline monolayer.

During the process of the cooling multi-step creep method, the molecular occupied area of the monolayer became fairly

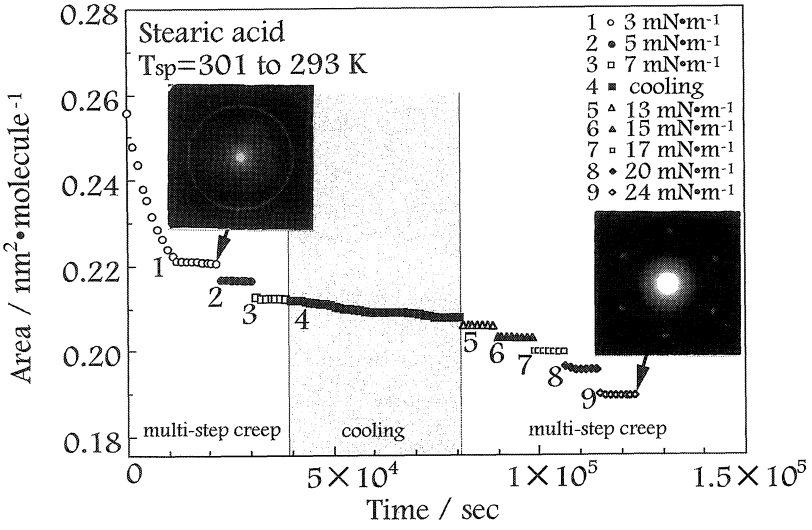

Fig. 5. Cooling multi-step creep behavior of the stearic acid monolayer

constant after a long area-creep process, even at a high surface pressure of 15 mN m^{-1} at which the monolayer prepared by the continuous compression method easily collapsed. Also, the ED pattern of the stearic acid crystalline monolayer prepared by the cooling multi-step creep method was the crystalline 6-spots. Therefore, it can be concluded that the crystallites in the monolayer prepared by the cooling multi-step creep method became larger in diameter than an electron beam diameter of 10 μm at least. This resulted in the formation of an apparent monodomain monolayer due to sintering behavior caused by cooling the monolayer below T_{α_c}.

Possible Mechanism for Formation of Structurally Regularized Monolayers by Cooling Multi-Step Creep Method. Table 1 summarizes the crystallographical regularities of the monolayers, that is, the magnitudes of crystallographical continuity (L_{lat}) and crystallographical distortion (D_{lat}), as evaluated from the (10) ED profiles of the monolayers prepared by the continuous compression method, the multi-step creep method and the cooling multi-step creep method, respectively. The crystallographical regularity of the monolayers in a lateral direction, that is, along the (10) direction was drastically increased by structural relaxation based on the step-wise alternating area creep and compression, and was further improved by the thermal treatment, as indicated by the comparison between multi-step creep method and cooling multi-step creep one. Figure 6 shows the schematic representation of the aggregation processes of the monolayer in the continuous compression method, the multi-step creep method or the cooling multi-step creep method. In the case of the continuous compression method, the 2-dimensional crystalline domains were gathered together by a continuous compression to a high surface pressure directly. Therefore, there might be not enough time to carry out sufficient structural relaxation for filling vacancies in the monolayer and also, to rearrange the molecular packing in the monolayer on the water surface into the defect-diminished or defect-free hexagonal packing which was the crystal system of the stearic acid monolayer at 293 K.[16] Since structural defects or vacancies were formed at the interfaces among monolayer domains during a continuous compression, as shown by Fig. 6a, the monolayer collapse might be induced by stress concentrations at structural defects or vacancies, resulting in the poor crystallographical regularity of the monolayer prepared by the continuous compression method. In other words, in the case of the continuous compression method, stress concentrations occurred at the domain boundary in the

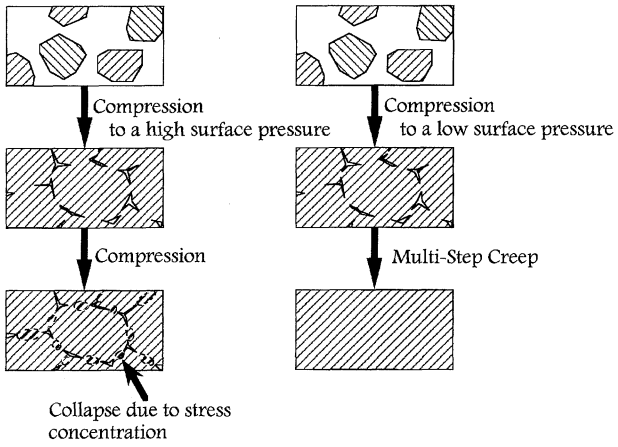

(a) continuous compression method (b) multi-step creep and cooling multi-step creep method.

Fig. 6. Schematic representation of the aggregation process of the monolayer by continuous compression method (a), multi-step creep, and cooling multi-step creep method (b).

monolayer, because the monolayer prepared by the continuous compression method showed the inhomogeneous aggregation structure and a compressing force could not propagate homogeneously in the monolayer. On the other hand, in the case of the multi-step creep method or the cooling multi-step creep method, there might be sufficient time for sufficient structural relaxation and molecular rearrangement during step-wise area-creep from a low surface pressure to a high surface pressure. Furthermore, in the case of the cooling multi-step creep method, it is apparent that the area creep at T_{sp} above T_{α_c} was effective for the structural relaxation because of the active thermal molecular motion at T_{sp} above T_{α_c}. Therefore, it seems reasonable to consider that the lateral crystallographical regularity of the monolayer prepared by the cooling multi-step creep method was drastically progressed compared with that prepared by the conventional continuous compression method.

Table 2 shows the longitudinal structural regularities of the LB films composed of the 30 monolayers, that is, the magnitudes of structural continuity (L_{long}) and structural distortion (D_{long}) along the direction perpendicular to the layer surface of the LB film. There values were evaluated from the SAXS profiles of the LB films prepared by the continuous compression method, the multi-step creep method and the cooling multi-step creep method, respectively. The stearic acid monolayers were transferred onto a hydrophobic sili-

Table 1. Crystallographical Regularities of the Monolayers Prepared by Continuous Compression, Multi-Step Creep, and Cooling Multi-Step Creep Method

Preparation method	Crystallographical distortion/% D_{lat}	Crystallographical continuity/nm L_{lat}
Continuous compression	5.0	6.2
Multi-step creep	3.1	22.9
Cooling multi-step creep	2.9	25.4

Table 2. Longitudinal Structural Regularities of the LB Films Prepared by Continuous Compression, Multi-Step Creep, and Cooling Multi-Step Creep Method

Preparation method	Structural distortion/% D_{long}	Structural continuity/nm L_{long}
Continuous compression	3.8	16.9
Multi-step creep	1.9	28.3
Cooling multi-step creep	1.3	45.2

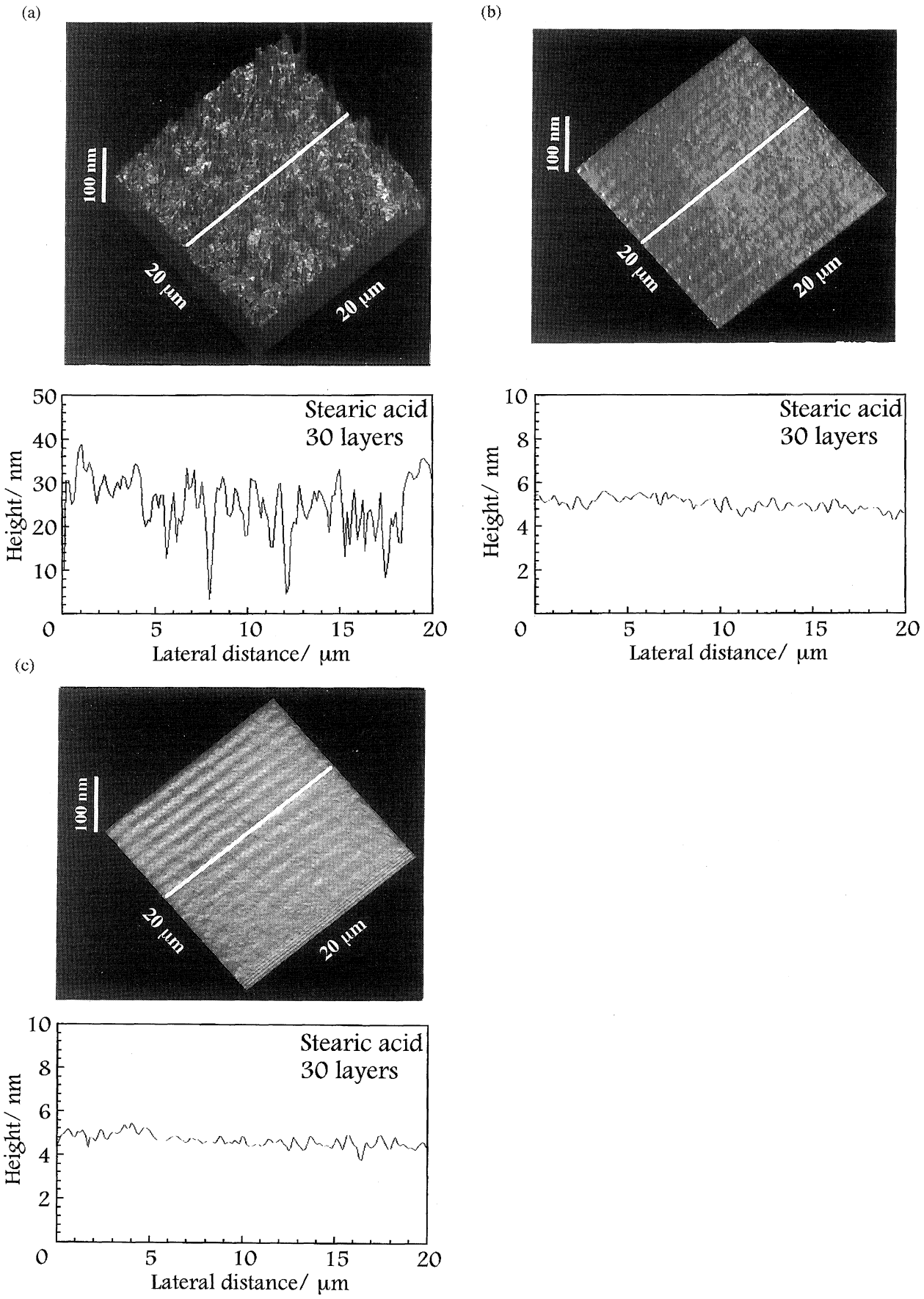

Fig. 7. AFM images of LB films prepared by continuous compression (a), multi-step creep (b), and cooling multi-step creep method (c). (a) Continuous compression method, (b) Multi-step creep method, (c) Cooling multi-step creep method.

conized substrate by the vertical dipping method: The transfer speed was 1 mm s^{-1} and the transfer ratios were always unity. Also, the SAXS profiles of the LB films were composed of the high-ordered reflection peaks of (001) whose layer spacings were agreed with a bilayer thickness of the stearic acid monolayer. This means that the stearic acid LB films were the well-ordered Y-type film. As shown in Table 2, the longitudinal structural regularity of the LB film showed a similar tendency to the lateral crystallographical regularity of the monolayer with respect to the monolayer preparation method. Also, Fig. 7 shows the AFM images of the LB films in a scan area of 20×20 μm and the height profile along the straight line, prepared by the continuous compression method (a), the multi-step creep method (b), and the cooling multi-step creep method (c), respectively. The surface morphologies of the LB film prepared by the multi-step creep method and the cooling multi-step creep method were fairly smooth and homogeneous, while that prepared by the continuous compression method was rough and heterogeneous. As mentioned before, since the monolayer prepared by the continuous compression method was "mechanically unstable", the monolayer prepared by the continuous compression method might be easily collapsed during the monolayer transfer process, resulting in the heterogeneous structure of the LB film. On the other hand, since in the case of the multi-step creep method and the cooling multi-step creep method, mechanically stable monolayers due to fairly low fractions of structural defects or vacancies were transferred onto the hydrophobic siliconized substrate, the surface morphology of the LB film should be fairly smooth and homogeneous. Hence, it is reasonable to conclude from Table 2 and Fig. 7 that the morphological roughness was apparently reflected in the structural regularity of the LB film. Therefore, the cooling multi-step creep method is extremely useful for the preparation of the highly structural regularized monolayers as well as the LB film waveguides in which a highly structural regularity is necessary.

Optical Waveguide Properties of LB Films. In order to construct an optical waveguide, it is necessary to control the thickness of the waveguide exactly, because an incident light beam of a optical wavelength is only permitted in the waveguide which satisfies the guide condition determined by the refractive index and the thickness. Since the LB technique can control the film thickness in a nm order, the LB film can be a possible candidate for the optical waveguide.

The stearic acid monolayer prepared in this study was in a crystalline state and the alkyl chains were in an almost *trans* conformation.[12] Since the thickness of the LB film composed of the 149 monolayers was ca. 330 nm, a TE_0 mode only might be able to propagate in the case of the He–Ne laser beam of 633 nm wavelength.

Figure 8 shows the waveguide length dependence of scattered light intensities for the stearic acid LB film waveguides prepared by the continuous compression method, the multi-step creep method and the cooling multi-step creep method, respectively. The instrumental noise due to incident light was cancelled by subtracting the light intensity of the blank

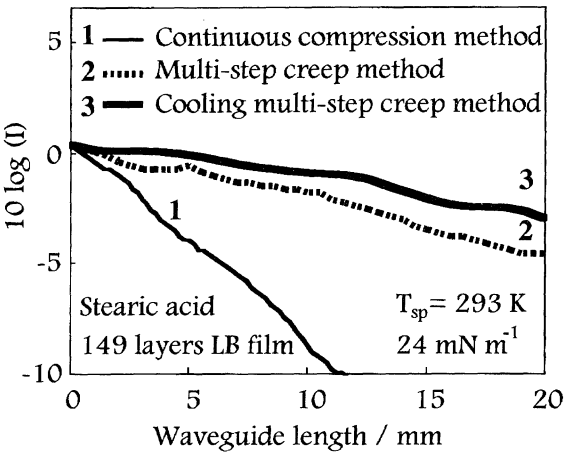

Fig. 8. Scattering light intensity from the LB film waveguides prepared by continuous compression, multi-step creep, and cooling multi-step creep method.

sample without the LB film waveguide from that of the optical waveguide. The scattered light intensity for the LB film waveguide prepared by the continuous compression method decreased remarkably with an increase of waveguide length. On the other hand, the scattered light intensity for the LB film waveguides prepared by the multi-step creep and the cooling multi-step creep methods decreased slightly with an increase of waveguide length, as shown by curves 2 and 3 in Fig. 8. Since the scattered light intensity corresponds to that of the propagated one, the optical propagation loss of the LB film waveguide could be calculated from the slope of the propagated length-scattered light intensity relationship,[17] as given by Eq. 1, where $I(x_1)$ and $I(x_2)$ were the scattered light intensities at the detector positions, x_1 and x_2, respectively.

$$N\ [\mathrm{dB\,cm^{-1}}] = \frac{-10\log\{I(x_2)/I(x_1)\}}{x_2 - x_1}. \quad (1)$$

Table 3 shows the propagation losses of the LB films prepared by the continuous compression method, the multi-step creep method and the cooling multi-step creep method, respectively. The propagation loss of the LB film waveguide was drastically decreased by using the preparation methods for the highly structurally regularized monolayers, that is, the multi-step creep method and the cooling multi-step creep method. The surface roughness of the LB film prepared by each creep method was fairly small and the uniformity of the LB film thickness was remarkable in comparison with the thicknesses of those prepared by the continuous compression method, as shown in Fig. 8. Since the surface morphology

Table 3. Propagation Losses of the LB Film Waveguides Constructed by Continuous Compression, Multi-Step Creep, and Cooling Multi-Step Creep Method Evaluated by Scattered Light Intensity Measurements

Preparation method	Propagation loss /dB cm^{-1}
Continuous compression	8.3
Multi-step creep	2.5
Cooling multi-step creep	1.6

of the LB film waveguide strongly affects the light propagation through the planar waveguide, the condition of the total reflection was broken down at the rough surface of the waveguides. Thus the guided light was largely scattered at the rough surface of the waveguide. Therefore, the difference of the propagation loss between LB film waveguides prepared by the multi-step creep method and by the cooling multi-step creep method could be explained by the surface roughness and the uniformity of the thickness of the LB film. Since Rayleigh scattering is strongly related to the structural fluctuations in the LB film and this might be a main factor for the propagation loss in the case of the fairly flat LB film waveguides, it can be concluded that the cooling multi-step creep method is one possible candidate for a low propagation loss LB film waveguide.

Conclusion

The cooling multi-step creep method can provide the defect-diminished crystalline monolayers by control of both the thermal molecular motion in the monolayer and the structural relaxation induced by the area-creep. LB film with a homogeneous surface morphology and a high structural regularity could be constructed by the deposition of the highly regularized monolayer prepared by a structurally regularized method such as the cooling multi-step creep method. The optical propagation loss of the LB film waveguide was decreased by improvement of the surface homogeneity and the structural regularity of the LB film. Therefore, the cooling multi-step creep method is extremely useful for construction of the LB film which needs highly structural regularity, such as the LB film waveguide.

This work was supported by a Grant-in-Aid for COE Research "Design and Control of Advanced Molecular Assembly Systems" (#08CE2005) from the Ministry of Education, Science, Sports and Culture. The authors thank Dr. Y. Oishi (Saga University) and T. Kuri (Kyushu University) for helpful discussions. One of us (M.Y.) is also grateful to Dr. H. Kikuchi (Kyushu University) for his help with waveguide measurements.

References

1 "Nonlinear Optical Properties of Organic Molecules and Crystals," ed by D. S. Chemla and J. Zyss, Academic Press, Orlando (1987).

2 A. Ulman, "An Introduction to Ultrathin Organic Films: from Langmuir–Blodgett to Self-Assembly," Academic Press, Boston (1991).

3 S. H. Ma, X. Z. Lu, J. Chen, K. Han, L. Y. Liu, Z. Huang, R. F. Cai, G. M. Wang, W. C. Wang, and Y. F. Li, *J. Phys. Chem.*, **100**, 16629 (1996).

4 H. Q. Li, Z. Q. Yao, R. H. Liu, G. Z. Tan, and X. D. Yu, *Chem. Lett.*, **1998**, 1205.

5 M. V. Martinez-Diaz, B. del Rey, T. Torres, B. Agricole, C. Mingotaud, N. Cuvillier, G. Rojo, and F. Agullo-Lopez, *J. Mater. Chem.*, **9**, 1521 (1999).

6 C. Bosshard, M. Kupfer, P. Gunter, C. Pasquier, S. Zahir, and M. Seifert, *Appl. Phys. Lett.*, **56**, 1204 (1990).

7 C. Bosshard, M. Kupfer, M. Florsheimer, and P. Gunter, *Thin Solid Films*, **210/211**, 153 (1992).

8 T. Kuri, Y. Oishi, and T. Kajiyama, *Trans. Mater. Res. Soc. Jpn.*, **15A**, 567 (1994).

9 T. Kuri, F. Hirose, Y. Oishi, K. Suehiro, and T. Kajiyama, *Langmuir*, **13**, 6497 (1997).

10 T. Kajiyama, N. Morotomi, M. Uchida, and Y. Oishi, *Chem. Lett.*, **1989**, 1047.

11 T. Kajiyama, Y. Oishi, M. Uchida, N. Morotomi, J. Ishikawa, and Y. Tanimoto, *Bull. Chem. Soc. Jpn.*, **65**, 864 (1992).

12 T. Kajiyama, Y. Oishi, M. Uchida, Y. Tanimoto, and H. Kozuru, *Langmuir*, **8**, 1563 (1992).

13 Y. Oishi, T. Kuri, Y. Takashima, and T. Kajiyama, *Chem. Lett.*, **1994**, 1445.

14 D. Hofmann and E. Walenta, *Polymer*, **28**, 1271 (1987).

15 R. Hosemann, *J. Appl. Phys.*, **34**, 25 (1963).

16 T. Kuri, Y. Oishi, and T. Kajiyama, *Bull. Chem. Soc. Jpn.*, **67**, 942 (1993).

17 W. Hickel, G. Appel, D. Lupo, W. Prass, and U. Scheunemann, *Thin Solid Films*, **210/211**, 182 (1992).